Finite Element Simulations in Electrochemistry. 2. Hydrodynamic Voltammetry

Nicholas P. C. Stevens and Adrian C. Fisher*

School of Chemistry, University of Bath, Claverton Down, Bath BA2 7AY, United Kingdom

Received: May 7, 1997; In Final Form: July 26, 1997[⊗]

A numerical strategy is reported based on the finite element method for simulating the mass transport limited current flowing at macro- and microelectrodes located within a rectangular channel cell. Specifically, simulations of a large planar, microband, and microstrip electrode are presented and the results compared to those predicted using alternative strategies. The finite element method is shown to be a flexible and efficient alternative to the previous strategies employed. The potential to extend finite element simulations to more complex geometries less suited to finite difference simulations is noted.

Introduction

The merits of hydrodynamic voltammetry using either macro- or microelectrodes have now been widely established,[1−7] for example, the exploitation of rapid flow over a microband electrode sited in a channel flow cell permits the monitoring of electrochemical events on the nanosecond time scale.[8] The application of such devices to elucidate kinetic and mechanistic properties of chemical systems relies on the ability to quantify the magnitude of the mass transport limited currents measured. It is therefore vital that efficient and flexible numerical strategies are available to the experimentalist.[9,10] Traditionally the approach of choice for the simulation of electrochemical phenomena has been based on finite difference techniques.[7−10] In this paper we explore an alternative approach for the simulation of electrochemical systems. Specifically we present theory and the results from the application of the finite element method (FE)[11,12] to the simulation of the mass transport limited currents flowing at an electrode sited in a channel flow cell. Previous reports in the academic literature of finite element techniques applied to the investigation of electrochemical processes have been somewhat restricted and fragmentary in nature.[13,14] Recently we have reported the application of the FE method to the simulation of electrochemical problems restricted to diffusion only, for a range of complex geometries.[15] In this paper we significantly expand this to address hydrodynamic systems.

Three electrode geometries were selected, (i) a macroelectrode (ii) a microband electrode,[8] and (iii) a microstrip electrode,[16] and each was situated within a channel flow cell (Figure 1). For each geometry the mass transport limited current/flow rate behavior calculated using the FE method was compared to that predicted using alternative finite difference methods. Good agreement was found between the results predicted using the FE method and those presented previously. Three potential advantages of the FE over the finite difference techniques were noted. First, FE simulations enable a direct steady-state solution to be obtained whereas the simulations presented previously for microband and microstrip geometries have relied on a time-marching approach. This is unnecessarily expensive computationally when only a steady-state solution is required. Second, previous simulations of hydrodynamic voltammetry have employed an analytical approximation of the solution velocity whereas here the flow profile is first calculated numerically for the appropriate geometry. Finally, although not exploited in this paper the finite element method provides a versatile tool to explore electrode geometries far more complex than those simulated previously. The ability to piece together elements of different shapes/sizes offers the opportunity to explore the electrochemical behavior of new hydrodynamic electrode systems not easily accessible using more traditional methods.

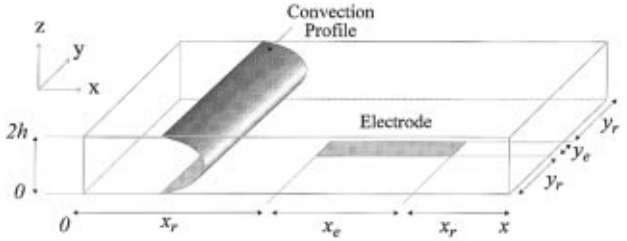

Figure 1. Schematic of the channel type flow cell.

Theory

In this section the theoretical model of the mass transport in the channel cell is developed. Three geometries are considered (Figure 1): case (i), the macroelectrode has y_e and x_e in excess of 0.4 cm, and y_r and x_r are of no importance computationally[18] and may be disregarded. For the microband (ii), y_e is microscopic, taken here to mean 50 μm or below, x_e is macroscopic, and y_r and x_r must be sufficiently large for the diffusion layer not to reach any of the cell walls except the rear wall at a distance sufficiently far from the electrode that the no flux boundary condition is valid. For geometry (iii) the constraints are identical but x_e is microscopic and y_e may be macroscopic. For all the geometries discussed, the total width of the cell in y is assumed to be large compared to that of y_e, to ensure that the flow profile above the electrode is not appreciably curved in y.

For the purposes of this paper we will consider the mass transport limited one-electron-transfer reaction under steady-state conditions.

$$A + e- \rightarrow B$$

If migration is neglected and only the V_x velocity component is significant, then the mass transport of species A to the electrode will be governed by

$$\frac{\partial C}{\partial t} = D\frac{\partial C^2}{\partial x^2} + D\frac{\partial C^2}{\partial y^2} + D\frac{\partial C^2}{\partial z^2} - V_x\frac{\partial C}{\partial x} = 0 \qquad (1)$$

* To whom correspondence should be addressed. E-mail: A.C.Fisher@bath.ac.uk. Tel: 44-1225-826-627. Fax: 44-1225-826-231.

[⊗] Abstract published in *Advance ACS Abstracts,* September 15, 1997.

S1089-5647(97)01529-0 CCC: $14.00

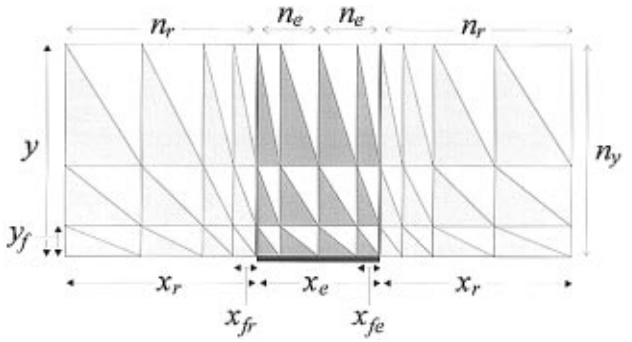

Figure 2. Grid used for two-dimensional convective−diffusive simulations, assembled from a mesh of triangular elements covering the region, with shading for illustration only.

TABLE 1

Geometries One and Two			
$y = 0$	$x_r < x < x_r + x_e$		$C = 0$
$y = 0$	$x < x_r$		$dC/dy = 0$
$y = 0$	$x > x_r + x_e$		$dC/dy = 0$
$y = 2h$	all x		$dC/dy = 0$
all y	$x = 0$		$dC/dy = 0$
all y	$x = 2x_r + x_e$		$dC/dy = 0$
Geometry Three			
$x_r < x < x_r + x_e$	$y_r < y < y_r + y_e$	$z = 0$	$C = 0$
$x < x_r$	all y	$z = 0$	$dC/dy = 0$
$x > x_r + x_e$	all y	$z = 0$	$dC/dy = 0$
$x_r < x < x_r + x_e$	$y < y_r$	$z = 0$	$dC/dy = 0$
$x_r < x < x_r + x_e$	$y > y_r + y_e$	$z = 0$	$dC/dy = 0$
all x	all y	$z = 2h$	$dC/dy = 0$
$x = 0$	all y	all z	$dC/dy = 0$
$x = 2x_r + x_e$	all y	all z	$dC/dy = 0$
all x	$y = 0$	all z	$dC/dy = 0$
all x	$y = 2y_r + y_e$	all z	$dC/dy = 0$

where C is the concentration, D is the diffusion coefficient, and x, y, and z are the coordinates of a point as defined in Figure 1.

In this paper we present simulations for the cases of one-, two-, and three-dimensional diffusion in the presence of one-dimensional convection. The finite element method is use to determine both the convective and diffusive properties of the system. The results of the simulations are demonstrated to agree with those presented previously using alternative methodology[8,16] for the chosen geometries.

The boundary conditions pertinent to the problems of interest are presented in Table 1.

To solve eq 1 for each geometry we use the finite element method.[11,12,15] This approach divides the cell into a continuous assembly of elements, within which the concentrations of each species are defined. Depending on the geometry and dimensionality of the problem, suitable grids may be defined.

Geometries One and Two. Figure 2 shows a schematic of an appropriate grid for two-dimensional convective diffusive problems. The grid is assembled from triangular elements, formed from the subdivision of a rectangular array, and expands from the edges of the electrode out to the edge of the simulated region, back to the center of the electrode from the edges, and from the lower wall of the simulation up to the upper wall. The algorithm giving the sizes of the elements is defined by the size of the first element to give a geometric series as reported previously.[15] Parameters of the form x or y indicate dimensions, and parameters of the form n_x represent the number of elements over a region, with the subscript indicating the region measured. The grid is normally constructed so as to be symmetrical about the center of the electrode.

Geometry Three. The three-dimensional grid used is formed by decomposing the volume under consideration first into cubes, as shown in Figure 3, and then subdividing each cube into five tetrahedrons, also shown at the top left.

For each geometry the method of solving the time-independent form of eq 1 is to set the integral of the concentration profile over the whole assembly of elements equal to zero. The general Galerkin form of eq 1 for the three-dimensional diffusional problem with one-dimensional convection is

$$\int\int_{V^e}\int N_i\left(\frac{\partial}{\partial x}\left(D_x\frac{\partial C^e}{\partial x}\right)+\frac{\partial}{\partial y}\left(D_y\frac{\partial C^e}{\partial y}\right)+\frac{\partial}{\partial z}\left(D_z\frac{\partial C^e}{\partial z}\right)-V_x\frac{\partial C^e}{\partial x}\right)dV = 0 \quad i = 1, 2..., n$$

where V^e is the volume of the element, and N_i is the interpolation function of the i noded element.[15] The solution of such problems with appropriate boundary conditions is outlined in refs 11 and 12.

The simulation produces the concentration distribution of species throughout the cell, from which we derive the current flowing using, for two dimensions,

$$I = FD_C[C]_{\text{Bulk}}\, y_e \sum_{i=1}^{ne}\frac{\delta x_i}{\delta z_i}\sum_{j=1}^{2}\frac{1}{2}[C]_{E(i,j)}$$

where $E(ne,2)$ is an array defined as part of the grid generation process, which numbers each square group of two triangles that lies above the electrode from 1 to ne and the two node points at the corners of each cube, δx_i and δz_i are the dimensions of these squares, and D_C is the diffusion coefficient (assuming diffusion is uniform in all directions). For three dimensions

$$I = FD_C[C]_{\text{Bulk}}\sum_{i=1}^{ne}\frac{\delta x_i \delta y_i}{\delta z_i}\sum_{j=1}^{4}\frac{1}{4}[C]_{E(i,j)}$$

where $E(ne,4)$ here numbers each cubic group of five tetrahedrons which lies above the electrode and the four node points at the corners of each cube, and δx_i, δy_i, and δz_i are the dimensions of these cubes.

Navier−Stokes Simulation. The simulation of the convection through a plane may be considered using isoparabolic eight noded elements, as shown in Figure 4, which are formed by considering the corner and midside nodes of a square. These elements are commonly used in the engineering community and have been shown to have desirable properties for fluid simulations. The basis function of such elements is of the form

$$\phi(x,y) = \alpha_1 + \alpha_2 x + \alpha_3 y + \alpha_4 xy + \alpha_5 x^2 + \alpha_6 y^2 + \alpha_7 xy^2 + \alpha_8 x^2 y$$

and intermediate values of the variables calculated are found according to their position within an element using the interpolation functions derived from this equation.[17]

The two-dimensional Navier−Stokes equations may be written in a dimensionless form, using the variables $x' = x/l$, $y' = y/l$, $u' = u/l$, $p' = p/(\rho u_0^2)$, and $v' = v/u_0$, representing the dimensionless x and y coordinates; u and v, the dimensionless velocities in x and y; and p, the dimensionless pressure. Also, l is a characteristic length and is the datum velocity. The dimensionless equations are

$$u'\frac{\partial u'}{\partial x'} + v'\frac{\partial u'}{\partial y'} = \frac{F_x l}{\rho {u_0}^2} - \frac{\partial p'}{\partial x'} + \frac{v}{u_0 l}\left(\frac{\partial^2 u'}{\partial x'^2} + \frac{\partial^2 u'}{\partial y'^2}\right)$$

$$u'\frac{\partial v'}{\partial x'} + v'\frac{\partial v'}{\partial y'} = \frac{F_x l}{\rho {u_0}^2} - \frac{\partial p'}{\partial y'} + \frac{v}{u_0 l}\left(\frac{\partial^2 v'}{\partial x'^2} + \frac{\partial 2v'}{\partial y'^2}\right)$$

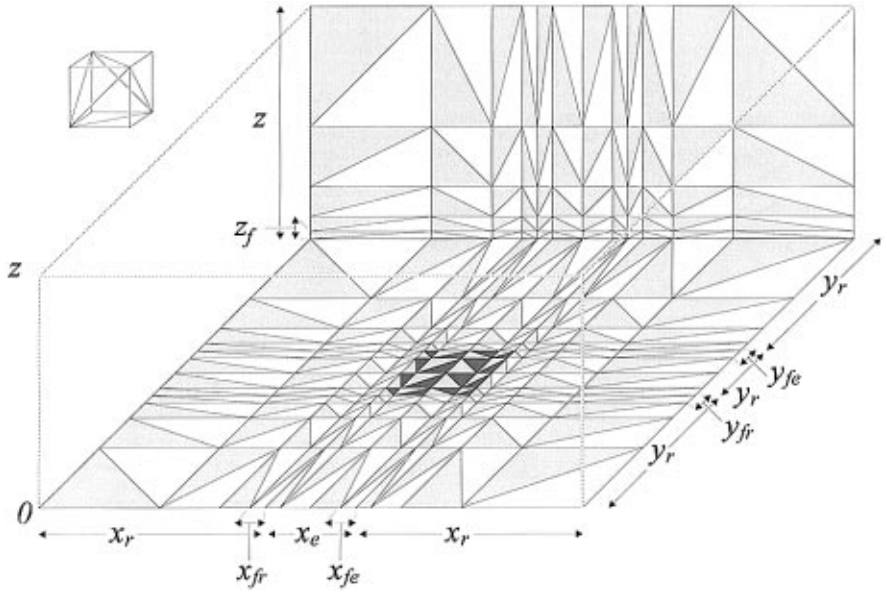

Figure 3. Schematic of the three-dimensional grid generation for a microstrip, assembled from a mesh of tetrahedral elements. The electrode is indicated by the darker shaded region, with the lighter shading for illustration only.

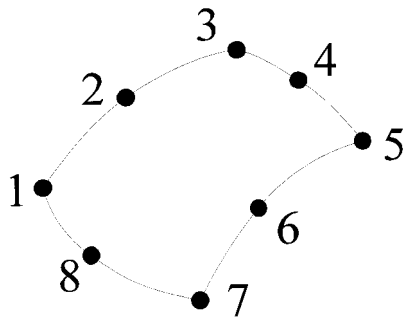

Figure 4. An eight-noded isoparabolic element used for convectional simulations.

and the continuity equation is

$$\frac{\partial u'}{\partial x'} + \frac{\partial v'}{\partial y'} = 0$$

From this point on the primes denoting normalized variables will be omitted. Also, the constants may be collected using $Re = u_0 l/\nu$, the Reynolds number, and $Fr = u_0/(gl)^{1/2}$, the Froude number of a flow, to give

$$u\frac{\partial u}{\partial x} + v\frac{\partial u}{\partial y} = \frac{l_{x1}}{Fr^2} - \frac{\partial p}{\partial x} + \frac{1}{Re}\left(\frac{\partial^2 u}{\partial x^2} + \frac{\partial^2 u}{\partial y^2}\right)$$

$$u\frac{\partial v}{\partial x} + v\frac{\partial v}{\partial y} = \frac{l_{x2}}{Fr^2} - \frac{\partial p}{\partial y} + \frac{1}{Re}\left(\frac{\partial^2 v}{\partial x^2} + \frac{\partial^2 v}{\partial y^2}\right)$$

where l_{x1} and l_{x2} are the direction cosines of the x and y global axes to the direction of the gravitational field.

The continuity equation remains:

$$\frac{\partial u}{\partial x} + \frac{\partial v}{\partial y} = 0$$

These three equations are coupled in the case of rotational flows, and must be solved simultaneously. Taking the variables to be given by the products of the shape functions and the matrices of nodal coordinates and following the practice of using a lower order function for evaluating the pressure rather than the other primitive variables

$$u = \sum_{i=1}^{i=n} N_i u_i, \quad v = \sum_{i=1}^{i=n} N_i v_i, \quad \text{and} \quad p = \sum_{i=1}^{i=m} M_i p_i,$$

where $n = 8$ and $m = 4$

and employing a Galerkin weighted residual technique

$$\sum_1^{ne}\int_{A^e} N_i\left[\sum_1^n N_k u_k \sum_1^n \frac{\partial N_j}{\partial x}u_j + \sum_1^n N_k v_k \sum_1^n \frac{\partial N_j}{\partial y}u_j + \sum_1^m \frac{\partial M_l}{\partial x}p_l - \frac{l_{x1}}{Fr^2} - \frac{1}{Re}\left(\sum_1^n \frac{\partial^2 N_j}{\partial x}u_j + \sum_1^n \frac{\partial^2 N_j}{\partial y^2}u_j\right)\right] \mathrm{d}A^e = 0$$

The second-order terms in this equation can be reduced, using Green's theorem as follows

$$\frac{1}{Re}\int_{A^e} N_i\left(\sum_1^n \frac{\partial^2 N_j}{\partial x}u_j + \sum_1^n \frac{\partial^2 N_j}{\partial y^2}u_j\right)\mathrm{d}A^e = \frac{1}{Re}\int_{\Gamma^e} N_i \sum_1^n \frac{\partial N_j}{\partial n}u_j \,\mathrm{d}s - \frac{1}{Re}\int_{A^e}\left[\frac{\partial N_i}{\partial x}\sum_1^n \frac{\partial N_j}{\partial x}u_j + \frac{\partial N_i}{\partial y}\sum_1^n \frac{\partial N_j}{\partial y}u_j\right]\mathrm{d}A^e$$

where Γ^edenotes the element surface. The terms arising from this surface will sum to zero on interelement boundaries and so must be retained for element edges on boundaries of the whole domain only. Using this method to simplify the second-order terms, the overall equation is found as given below. Note that all summations are implied, for subscripted variables, with $l = 1...4$, $j = 1...8$, $k = 1...8$, $i = 1...$number of nodes.

$$\sum_1^{ne}\int_{A^e}\left(N_i N_k u_k \frac{\partial N_j}{\partial x}u_j + N_i N_k v_k \frac{\partial N_j}{\partial y}u_j + N_i \frac{\partial M_l}{\partial x}p_l - N_i\frac{l_{x1}}{Fr^2} + \frac{1}{Re}\left(\frac{\partial N_i}{\partial x}\frac{\partial N_j}{\partial x}u_j + \frac{\partial N_i}{\partial y}\frac{\partial N_j}{\partial y}u_j\right)\right)\mathrm{d}A^e - \int_{\Gamma_1^e}\frac{1}{Re}N_i\frac{\partial N}{\partial n}u_j \,\mathrm{d}\Gamma - \int_{\Gamma_2^e}\frac{1}{Re}N_i\left(\frac{\partial u_j}{\partial n}\right)\mathrm{d}\Gamma = 0$$

where Γ_2^e is a boundary over which a gradient type boundary condition is specified. The complimentary equation in the y

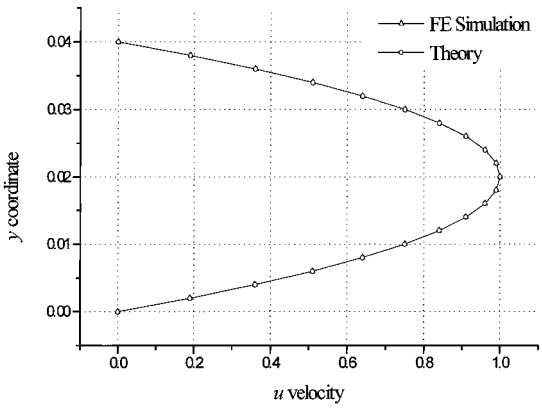

Figure 5. Simulated and theoretical convective profile for a channel system.

direction is given by interchanging x and y and u and v in the above equation.

The continuity equation in terms of the shape functions and nodal vectors is

$$\sum_{1}^{ne}\int_{A^e} M_i\left(\frac{\partial N_j}{\partial x}u_j + \frac{\partial N_j}{\partial y}v_j\right)\mathrm{d}A^e = 0$$

The pressure is evaluated using a lower order function than the other two primitive variables and depends only on corner nodes of the eight noded elements used.

Results and Discussion

For the purposes of this paper convective simulations were restricted to geometries and pressures to produce Reynolds numbers < 100. In all cases the well-documented parabolic flow profile is generated.

The parabolic convection profile given by the finite element simulations, as shown in Figure 1, was compared to the analytical profile for fully developed laminar flow between semi-infinite parallel plates, which is described by the equation

$$u_x = u_0(1 - (h - y)^2/h^2)$$

where u_x is the velocity in the x direction, u_0 is the velocity at the center of the channel, and $2h$ is the height of the channel. Figure 5 shows the almost perfect agreement between the simulations presented and the analytical theory. A regular grid with 10 isoparabolic elements in both x and y, with $x = 1$ cm and $y = 0.04$ cm, was used, with a center velocity of 1 cm s^{-1}.

One-Dimensional Diffusion and One-Dimensional Convection. For an electrode which is sufficiently large as to make edge effects insignificant,[18] the Levich equation has been shown to predict the current flowing as a function of flow rate

$$I_{\mathrm{lim}} = 0.925nF[C]_{\mathrm{Bulk}}\, x_e^{2/3} w D^{2/3}\left(\frac{V_f}{h^2 d}\right)^{1/3}$$

where $V_f = 4u_0hd/3$, d is the width of the cell in y, w is equivalent to y_e, h is the half-height of the cell in z, x_e is the length of the electrode, D is the diffusion coefficient, and $[C]_{\mathrm{Bulk}}$ is the bulk concentration.

Figure 6 shows the agreement between the simulations presented, eq 2, and results from a finite difference algorithm.[8] This close agreement demonstrates the validity of the finite element method.

The results shown are for a macroelectrode of dimensions $x_e = 0.4$ cm, $h = 0.02$ cm, and $x_r = 0.4$ cm, and with $D = 10^{-5}$ cm^2 s^{-1} and $[C]_{\mathrm{Bulk}} = 10^{-5}$ M dm^{-3}. The finite element

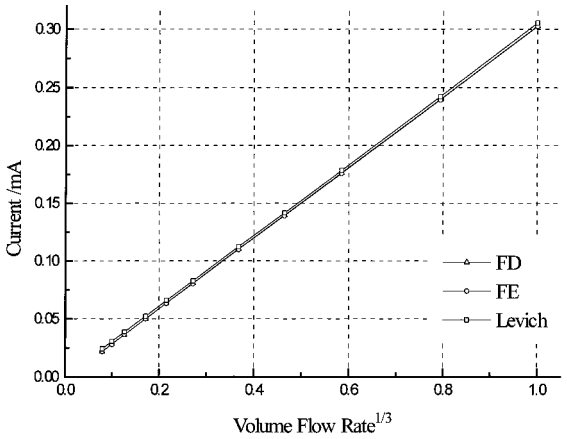

Figure 6. Graph showing simulations for a channel electrode and Levich equation.

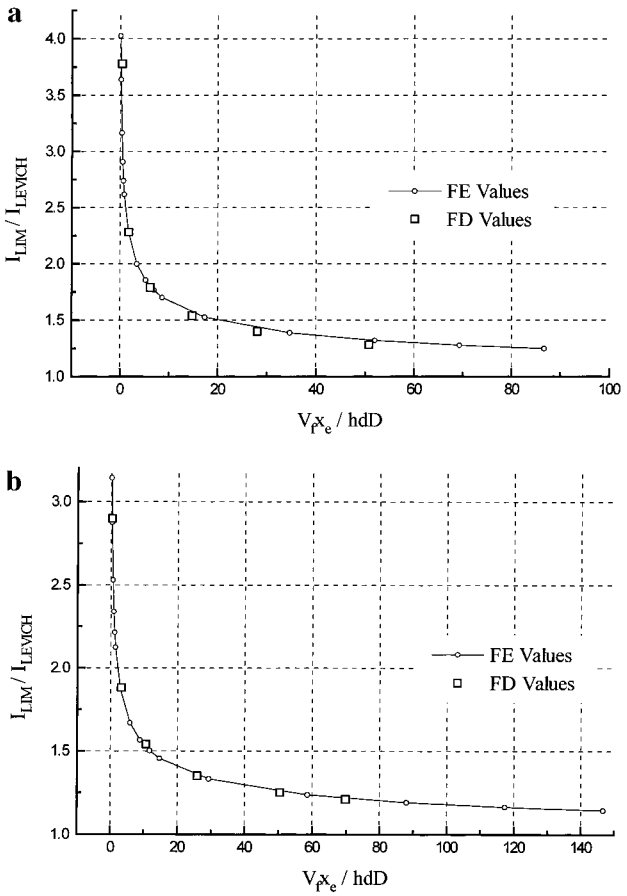

Figure 7. (a) Ratio of microband current for Levich current for a microband of size $x_e = 0.000\,65$ cm. (b) Ratio of microband current to Levich current for a microband of size $x_e = 0.0011$ cm.

simulations used parameters $n_y = 30$, $n_e = 20$, $n_r = 20$, $y_f = 2 \times 10^{-6}$ cm, $x_{fr} = 2 \times 10^{-6}$ cm, and $x_{fe} = 2 \times 10^{-6}$ cm. The finite difference simulations used a regular grid of 400 by 400 nodes over the same area.

Two-Dimensional Diffusion and One-Dimensional Convection. Previous approaches to problems of this type have relied on iterative techniques which are necessarily time consuming. Implementation of the finite element method enables the steady-state solution of the convection−diffusion problems presented without iteration.

As stated previously the influence of axial diffusion only becomes significant as the ratio $V_f x_e/hdD$ becomes small, and its influence may be measured by a plot of the ratio of the transport limited current over that predicted by the Levich equation, against $V_f x_e/hdD$. Figure 7 shows a comparison

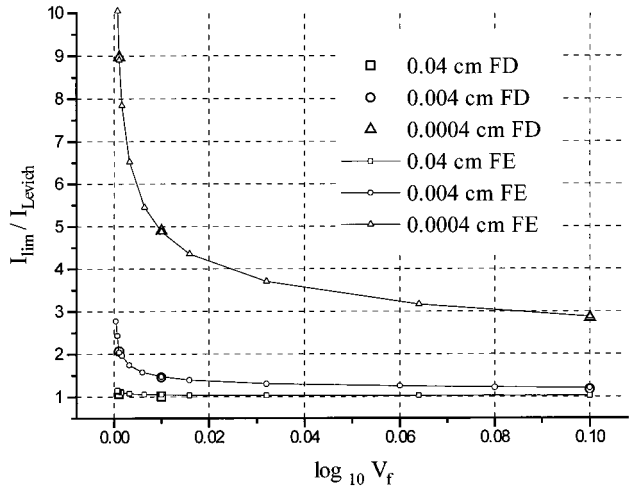

Figure 8. Ratios of simulated microstrip current to Levich current.

between the results of finite element simulations and previous finite difference simulations.[8] The parameters used for these simulations were $n_y = 20$, $n_r = 18$, $n_e = 20$, $h = 0.02$ cm, $x_r = 0.4$ cm, x_e varies as indicated, $x_{fe} = 5 \times 10^{-6}$ cm, $x_{fr} = 5 \times 10^{-6}$ cm, $y_f = 5 \times 10^{-6}$ cm, $D = 10^{-5}$ cm^2 s and $[C]_{Bulk} = 10^{-5}$ M dm^{-3}. u_0 varies so as to give a range of values for $V_f x_e/hdD$.

The Levich equation neglects diffusion in the plane of the electrode and thus underestimates the current where axial diffusion becomes significant. The relative contribution to the overall mass transport to the microband electrode of axial diffusion is greatest where the flow rate is low, as the diffusion layer is then allowed to extend furthest from the electrode in the x direction. This arises since the enhancement in mass transport to the electrode is mainly concentrated at the edges of the electrode and the smaller the electrode, the greater the portion of which will lie within the regions where the x diffusion is significant. The effect where the flux to an electrode of suitably small size is dominated by the flux to the edges of the electrode has become known as the "edge effect" and is characteristic of microelectrodes.[18]

Three-Dimensional Diffusion and One-Dimensional Convection. For the microstrip geometry the size of the electrode in the y direction is sufficiently small so that diffusion in y also becomes important in the overall mass transport to the electrode. The enhancement of the mass transport may again be observed as the ratio I_{lim}/I_{Levich}. Figure 8 shows the variation of I_{lim}/I_{Levich} with log V_f for microstrips of a range of widths and length 0.04 cm.

Again it can be seen that decreasing the flow rate allows the influence of diffusion to become more significant, as does narrowing the electrode. The parameters used for these simulations were $x_r = 0.4$, x_e varies as shown, $y_r = 0.1$ cm, $y_e = 0.0004$ cm, $z = 0.04$ cm, $n_{xr} = 9$, $n_{xhe} = 9$, $n_{yr} = 8$, $n_{ye} = 8$, $n_z = 18$, $z_f = 1 \times 10^{-5}$ cm, $x_{fe} = 8 \times 10^{-5}$ cm, $x_{fr} = 1 \times 10^{-5}$ cm, $y_{fe} = 2 \times 10^{-5}$ cm, $y_{fr} = 6 \times 10^{-6}$ cm, $D = 10^{-5}$ cm^2 s^{-1} and $= 10^{-5}$ M dm^{-3}.

Conclusion

The finite element technique is a valuable method for simulating the steady-state current flowing in a channel cell. Specifically, this method enables the solution of one- and two-dimensional convective−diffusional problems in a single computational operation. The ability to solve two- and three-dimensional steady-state problems without iteration offers a significant enhancement in computational efficiency. It is also apparent from the previous applications of the finite element technique[11,12] that this technique is particularly suited to complex geometries. Further developments of our strategy will include the adaptation of the technique to allow the development of novel hydrodynamic systems which cannot be precisely described analytically.

Acknowledgment. We thank the EPSRC for studentship 957 00 361 for N.S. and the Nuffield Foundation for supporting this research.

References and Notes

(1) Blaedel, W. J.; Olson, C. L.; Sharma, L. R. *Anal. Chem.* **1963**, *35*, 2100.
(2) Blaedel, W. J.; Klatt, L. N. *Anal. Chem.* **1966**, *38*, 879.
(3) Compton, R. G.; Unwin, P. R. *J. Electroanal. Chem.* **1986**, *206*, 57.
(4) Compton, R. G.; Sealy, G. R. *J. Electroanal. Chem.* **1983**, *145*, 35.
(5) Singh, T.; Dutt, J. *J. Electroanal. Chem.* **1985**, *182*, 259.
(6) Moldoveanu, S.; Anderson, J. L. *J. Electroanal. Chem.* **1984**, *175*, 67.
(7) Anderson, J. L.; Moldoveanu, S. *J. Electroanal. Chem.* **1984**, *179*, 107; 119.
(8) Compton, R. G.; Fisher, A. C.; Wellington, R. G.; Dobson, P. J.; Leigh, P. A. *J. Phys. Chem.* **1993**, *97*, 10410.
(9) Britz, D. *Digital Simulation in Electrochemistry*; Springer-Verlag: Berlin, 1981.
(10) Compton, R. G.; Pilkington, M. B. G.; Stearn, G. M. *J. Chem. Soc, Faraday Trans. 1* **1988**, *84* (6), 2155−2171.
(11) Ziekiewicz, O. C. *The Finite Element Method in Engineering Science*, 2nd ed.; McGraw-Hill: New York, 1977.
(12) Baker, A. J. *Finite Element Computational Mechanics*, 1st ed.; McGraw-Hill: New York, 1983.
(13) Penczek, M.; Stojek, Z.; Osteryoung, J. *J. Electroanal. Chem.* **1984**, *170*, 99.
(14) Penczek, M.; Stojek, Z.; Osteryoung, J. *J. Electroanal. Chem.* **1984**, *181*, 83.
(15) Stevens, N. P. C; Hickey, S. J.; Fisher, A. C. *An. Quim.*, in press.
(16) Aixill, W. J.; Fisher, A. C.; Fulian, Q. *J. Phys. Chem.* **1996**, *100*, 14067−14073.
(17) Taylor, C.; Hughes, T. G. *Finite Element Programming of the Navier−Stokes Equations*, 1st ed.; Pineridge Press: Swansea, 1981.
(18) Aoki, K.; Tokuda, K.; Matsuda, H. *J. Electroanal. Chem.* **1987**, *230*, 61−67.